# Pseudocapacitive gels based on conjugated polyelectrolytes thickness and ion diffusion limitations

Vázquez, Ricardo Javier; Quek, Glenn; Jiang, Yan; Rui Peng, Benjamin Yip; McCuskey, Samantha R.; Ohayon, David; Kundukad, Binu; Wang, Xuehang; Bazan, Guillermo C.

**DOI**
10.1039/d3ta02820h

**Publication date**
2023

**Document Version**
Final published version

**Published in**
Journal of Materials Chemistry A

Journal of Materials Chemistry A

ROYAL SOCIETY OF CHEMISTRY

PAPER

View Article Online
View Journal





Cite this: DOI: 10.1039/d3ta02820h

# Pseudocapacitive gels based on conjugated polyelectrolytes: thickness and ion diffusion limitations†

Ricardo Javier Vázquez, ‡[ab] Glenn Quek,‡[b] Yan Jiang,[b] Benjamin Yip Rui Peng,[b] Samantha R. McCuskey,[bc] David Ohayon,[b] Binu Kundukad,[c] Xuehang Wang[d] and Guillermo C. Bazan *[abc]

Conjugated polymer hydrogels (CPHs) are emerging pseudocapacitive materials capable of forming redox-active hydrogels. Current efforts focus on increasing their areal capacitance ($C_{Areal}$) and cycling stabilities by using binders tolerant to $H_2SO_4$-based electrolytes, while alternatives in more environmentally friendly electrolytes underperform due to low-capacity values. Herein, we demonstrate that it is possible to use conjugated polyelectrolyte (CPE), namely CPE-K, to create a single-component binder-free pseudocapacitive gel in environmentally friendly electrolytes (2 M: NaCl, $MgCl_2$, and $MgSO_4$), with $C_{Areal}$ 1.9 times larger than those reported for single-component binder-free CPHs. The resulting pseudocapacitive gel exhibited $C_{Areal}$ (523 mF cm$^{-2}$ at 0.25 mA cm$^{-2}$) scalable with its thickness in NaCl electrolytes, providing an attractive solution to improve the capacitance of devices while maintaining a minimal charge-collecting electrode surface footprint. In addition, the CPE-K gel demonstrates 86% capacitance retention after 100 000 cycles at 10 mA cm$^{-2}$, which is higher than those reported for conventional state-of-the-art conjugated polymers. Electrochemical characterization revealed that $C_{Areal}$ at all cycling rates tested is proportional to $d_{Thk}$ up to 750 μm, primarily due to facile ionic diffusion within the 3D conductive network of the gel. Thicker electrodes ($d_{Thk}$ = 1250 μm) can be operated at a rate of 15 mA cm$^{-2}$ with minimal capacity loss. These results demonstrate the potential applications of self-doped CPE gels in designing the next generation of multi-functional electrochemical energy storage and conversion technologies for targeting high energy and power density applications.

Received 12th May 2023
Accepted 10th August 2023

DOI: 10.1039/d3ta02820h

rsc.li/materials-a

## 1. Introduction

Pseudocapacitors deliver intermediate power and energy densities to batteries and electrical double-layer capacitors (EDLC).[1–8] The fast charge storage capabilities in pseudocapacitors occur *via* a combination of near-surface faradaic redox reactions concomitant to the interaction with stabilizing counterions.[6,8] However, the successful implementation of pseudocapacitive devices calls for materials that allow low-cost and scalable fabrication, while maintaining a large electroactive surface area (EASA).[2,9,10] To this end, conjugated polymers (CPs) offer attractive properties, including economic viability, mechanical flexibility, and a diverse and readily available set of molecular structures for performance optimization.[11–16] However, optimizing ionic conductivity and electrolyte accessibility in CP-based pseudocapacitors is still needed to maximize pseudocapacitance.[6,17–19]

Conductive polymer hydrogels (CPHs) are gaining interest as pseudocapacitive electrode materials due to specific physico-electrochemical properties that are difficult to achieve with traditional CP thin films.[9] In particular, CPHs can exhibit a large EASA when an interconnected morphology is present, leading to useful ionic and electrical conductivities and competitive capacitance per unit of area of the charge-collecting working electrode (areal capacitance, $C_{Areal}$).[20,21] Relevant examples include single-component CPHs based on polyaniline (PANI; $C_{Areal}$ = 270 mF cm$^{-2}$ at 0.5 mA cm$^{-2}$)[22] and PEDOT ($C_{Areal}$ = 120 mF cm$^{-2}$ at 0.5 mA cm$^{-2}$),[23] see Table 1. Improvements in the $C_{Areal}$ and the overall pseudocapacitive performance of CPHs based on PANI, PEDOT, and other CP were achieved by creating multi-component CPHs through various additives, such as graphene, inorganic materials, phytic acid, polyvinyl alcohol (PVA), or acrylic acid, among others.[10,24–26] These additives

[a]Institute for Functional Intelligent Materials, National University of Singapore, 117544, Singapore. E-mail: chmbgc@nus.edu.sg

[b]Departments of Chemistry and Chemical & Biomolecular Engineering, National University of Singapore, Singapore 119077, Singapore

[c]Singapore Centre for Environmental Life Sciences Engineering, Nanyang Technological University, Singapore 639798, Singapore

[d]Department of Radiation Science and Technology, Delft University of Technology, Delft 2629 JB, The Netherlands

† Electronic supplementary information (ESI) available. See DOI: https://doi.org/10.1039/d3ta02820h

‡ These authors contributed equally.

Table 1 Summary of CPH pseudocapacitive systems for energy storage applications

| Active material | Electrolyte | Capacitance[a] (mF cm$^{-2}$) | $\langle J \rangle$[b] (mA cm$^{-2}$) | Stability[c] | $d_{Thk}$[d,c] (μm) |
|---|---|---|---|---|---|
| Single-component CPH | | | | | |
| CPE-K* | 2 M NaCl | 90 | 0.5 | 96%/10 K cycles | 250 |
| CPE-K* | 2 M NaCl | 208 | 10 | 86%/100 K cycles | 750 |
| CPE-K* | 2 M NaCl | 523 | 0.25 | 86%/100 K cycles | 1250 |
| CPE-K[2] | MSBM + $Mg^{2+}$ | 72 | 2.5 | 76%/100 K cycles | 250 |
| PANI[22,40] | 1 M $H_2SO_4$ | 271 | 0.5 | 83%/10 K cycles | N/A |
| PEDOT[23] | PVA/$H_2SO_4$ | 120 | 0.5 | 82.5%/5 K cycles* | 100 |
| PPy[41] | PVA-$H_3PO_4$ | 210 (F g$^{-1}$) | 10 (A g$^{-1}$) | 31%/4 K cycles | N/A |
| Multiple-component CPH | | | | | |
| CPE-K/Graphene[9] | SBM + $Mg^{2+}$ | 80 | 0.25 | 85%/1 K cycles | 250 |
| PANI/Graphene[17] | 1 M $H_2SO_4$ | 578 | 0.5 | 97%/10 K cycles | N/A |
| PPy/Fe-PAA[25] | Fe-PAA | 2033 | 2 | 90%/4 K cycles | 1000 |
| PEDOT/PANI[42] | PVA/$H_2SO_4$ | 740 | 6.7 | N/A | N/A |
| PEDOT : PSS/PVA[43] | 1 M $H_2SO_4$ | 128.9 | 0.5 | 90%/10 K cycles | 1500 |
| PEDOT/PANI[23] | PVA/$H_2SO_4$ | 240 | 0.5 | 82.5%/5 K cycles | 100 |
| PPy/$TiO_2$/GO[27] | 1 M $NaSO_4$ | 300 (F g$^{-1}$) | 0.5 (A g$^{-1}$) | 90%/3 K cycles | N/A |
| PPy/ATA[41] | PVA-$H_3PO_4$ | 500 (F g$^{-1}$) | 10 (A g$^{-1}$) | 31%/4 K cycles | N/A |

[a] Values are represented in terms of areal capacitance ($C_{Areal}$ = mF cm$^{-2}$). [b] Current density ($J$ = mA cm$^{-2}$) unless indicated otherwise. [c] Stability refers to the capacitance retention upon multiple cycles. [d] $d_{Thk}$ refers to the thickness of the CPE-K gel. SBM refers to Shewanella Basal Medium. Polyaniline (PANI), polypyrrole (PPy), polyvinyl alcohol (PVA), and this work*.

improve the mechanical stability, conductivity, and redox-active sites of the resulting multi-component CPHs.[10,24–27] High electrical conductivity has also been achieved by chemical doping the CPH material using acids, such as $H_2SO_4$.[28,29] Thus, opportunities exist for developing high-performance pseudocapacitive CPHs that require no additives and are compatible with environmentally benign electrolyte solutions.

Conjugated polyelectrolytes (CPEs) are a particular class of CPs bearing pendant side chains with ionic functionalities.[2,9,30,31] Of relevance is poly[2,6-(4,4-bis-potassium butanesulfonate-4*H*-cyclopenta-[2,1-b; 3,4-b′]-dithiophene)-*alt*-4,7-(2,1,3-benzothiadiazole)] (CPE-K, see Fig. 1), a self-doped, p-type CPE that can self-assemble into a hydrogel with pseudocapacitive properties when dispersed in water.[2,9,32–35] Of relevance is that the mechanical and electrochemical properties of CPE-K hydrogels can be tuned by the identity of the electrolyte solutions.[31,36,37] For example, improvements in capacitance and cycling stability were demonstrated by creating two-component CPE-K/2D-electrolyte gels with a thickness of 250 μm. The 2D-graphene electrolyte increased capacitance retention from 40% to 85% of the initial $C_{Areal}$ (78 mF cm$^{-2}$ at 0.25 mA cm$^{-2}$) after 1000 cycles.[9] Moreover, increasing the molecular weight ($M_n$) from 19 kDa to 32 kDa has also been shown to lead to greater stability without the need for 2D electrolytes, ultimately retaining 76% of the initial $C_{Areal}$ (82 mF cm$^{-2}$ at 2.5 mA cm$^{-2}$) after 100 000 charge/discharge cycles (see Table 1).[2] A higher $M_n$ most reasonably promotes interchain contacts, resulting in a mechanically more robust percolated 3D conductive network and higher tolerance to volumetric changes upon cycling.[2,9,10,35,38,39]

In this contribution, we show that the pseudocapacitive and mechanical properties of single-component CPE-K gels are improved in traditional aqueous electrolyte solutions, namely 2 M NaCl, 2 M $MgCl_2$, and 2 M $MgSO_4$, relative to previously investigated biocompatible electrolytes. We also identify/investigate how the pseudocapacitive performances of CPE-K gels are affected by increasing thickness ($d_{Thk}$) from 250 to 1250 μm *via* increments in mass loading of active material. Electrochemical characterization reveals that $C_{Areal}$ scales proportionally to thickness, reaching values as high as 523 mF cm$^{-2}$, which is 1.9 times higher than those reported for state-of-the-art single-component binder-free CPHs in $H_2SO_4$-containing electrolytes (Table 1).[22] Furthermore, CPE-K gels retained over 86% (180 mF cm$^{-2}$) of their initial capacitance after 100

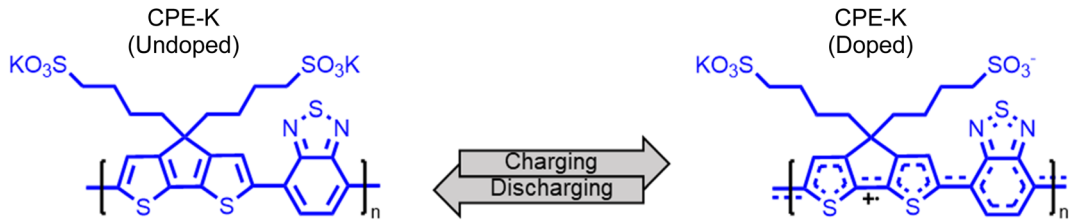


Fig. 1 Pseudocapacitive mechanism of the self-doped p-type CPE-K. Left: undoped (neutral; discharged) conjugated polyelectrolyte. Right: doped (oxidized; charged) CPE-K with stored positive charges compensated by anions from the electrolyte solution.

 

000 charge/discharge cycles at 10 mA $cm^{-2}$. Another relevant feature of our work is that CPE-K gels achieve state-of-the-art performances in aqueous and environmentally friendly electrolytes, a feature often overlooked in the performance race. We envision that our work will stimulate further consideration of self-doped CPE gels for enabling electrochemical energy storage and conversion technologies.[44,45]

## 2. Results and discussion

Relevant physico-electrochemical properties of CPE-K gels, namely mechanical robustness, pseudocapacitive window, $C_{Areal}$, and ionic diffusion, improve when $Mg^{2+}$ is added to a biocompatible electrolyte.[2,9] Historically, such electrolytes were based on phosphate buffers with ionic strength <1 M and were chosen for operating under biocompatible conditions with *S. oneidensis*.[32,33] Therefore, we examined the impact of using conventional electrolytes (NaCl, $MgCl_2$, and $MgSO_4$) at higher concentrations (2 M), to better reflect the traditional testing conditions of pseudocapacitive materials. We first carried out rheological measurements on 100 μL of 20 mg $mL^{-1}$ CPE-K gels (after ion exchange, see Methods) to investigate the effects of the electrolytes on the gel's mechanical properties.[2,37] In principle, rheology informs about the material's solid (elastic; $G'$) and liquid (viscous; $G''$) behavior.[46,47] As shown in Fig. 2A, $G'$ and $G''$ values are independent of frequency and $G' > G''$ across the measured frequency range, indicating that all gels exhibit solid-like characteristics regardless of the electrolyte.[37,48] Gels equilibrated in 2 M NaCl, $MgCl_2$, and $MgSO_4$ solutions showed average $G'$ values of 34 kPa, 38 kPa, and 42 kPa, respectively. These $G'$ values are approximately one order of magnitude higher than previously reported values for CPE-K gels in electrolyte solutions with ionic strength <1 M, highlighting the importance of electrolyte selection for rigidifying mechanical properties.[2,31] Note that the physical aspect of the hydrogel changes after ion exchange with the reservoir of the electrochemical cell (Fig. S1 and S2†), consistent with the higher $G'$ values reported in previous studies. This could be attributed to the effect of the highly concentrated electrolyte solution in exchanging the charge-compensating cation, enabling finer structural control of the CPE-K solution behavior.[31]

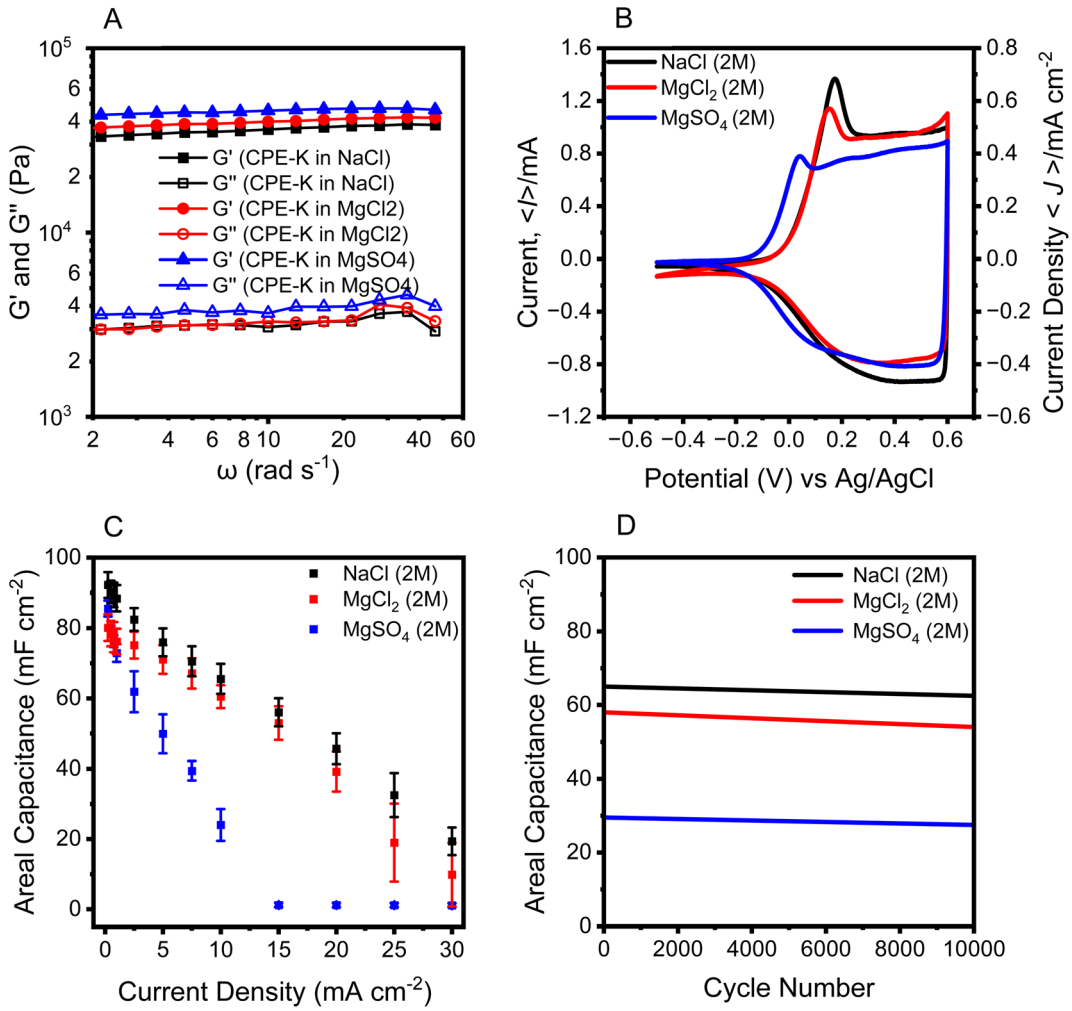


Fig. 2 Physical and electrochemical characterization of 20 mg $mL^{-1}$ CPE-K gels with 250 μm thickness in 2 M NaCl, 2 M $MgCl_2$, and 2 M $MgSO_4$: (A) rheological measurements; (B) cyclic voltammetry (CV) measurements at 5 mV $s^{-1}$, (C) areal capacitance in mF $cm^{-2}$ at different current densities ($\langle J \rangle$); (D) representative cycling stability characterization at 10 mA $cm^{-2}$. Measurements were carried out in ambient conditions.

The electrochemical response of CPE-K gels ($d_{Thk} = 250$ μm) was examined in 2 M NaCl, $MgCl_2$, and $MgSO_4$ *via* cyclic voltammetry (CV) using a 3-electrode setup using a 2 $cm^2$ CPE-K-coated Au working electrode, as described previously.[32,34] CV measurements were carried out daily at a rate of 5 mV $s^{-1}$ until the traces stabilized (2–4 days) to demonstrate equilibration of ion exchange with the electrolyte solution in the reservoir, see Fig. S3.† [9] The potential window was confined from −0.5 V to +0.6 V (all electrochemical measurements are reported *vs.* Ag/AgCl 3 M KCl) to avoid oxidation and irreversible electrochemical reactions of the working electrode.[2,49] As shown in Fig. 2B, CV curves of the CPE-K gel in all electrolytes display quasi-rectangular shapes with oxidation peaks at 0.05 V ($MgSO_4$) or 0.18 V (NaCl and $MgCl_2$), indicative of pseudocapacitive characteristics.[4,6,32] The CV traces are symmetric along the *x*-axis with coulombic efficiencies (CE) ~1 for all three electrolytes, as determined by dividing the charge ($Q$) of the discharge process over that of the charging process, suggesting high electrochemical reversibility, see Fig. S4 and S5.† [50,51] Of note is that the current peak maxima ($\langle I \rangle_p$) of the CV followed the trend of NaCl, $MgCl_2$, and $MgSO_4$, regardless of the scan rate used. For instance, the $\langle I \rangle_p$ for the NaCl, $MgCl_2$, and $MgSO_4$ electrolytes is 1.4 mA, 1.2 mA, and 0.8 mA, respectively, at 5 mV $s^{-1}$.

The pseudocapacitive performances of the CPE-K gels were examined using galvanostatic charge/discharge (GCD) measurements. GCD cycles were performed to determine $C_{Areal}$ values for CPE-K gels under different conditions using eqn (1):

$$C_{Areal} = I \times \Delta t/a \times \Delta V \quad (1)$$

where $I$ is the constant discharge current, $\Delta t$ is the discharge time, $a$ is the working electrode area, and $\Delta V$ is the potential operation window excluding the voltage drop ($IR_{drop}$). The $\Delta V$ range was set between +0.2 and +0.6 V.[32] At low cycling rates, the $C_{Areal}$ values converge to ~90 mF $cm^{-2}$ for the three electrolytes, see Fig. 2C and Table S1.† However, at rates up to 30 mA $cm^{-2}$, the $C_{Areal}$ values followed the trend NaCl > $MgCl_2$ > $MgSO_4$. For instance, at 10 mA $cm^{-2}$, the $C_{Areal}$ in NaCl is 65 mF $cm^{-2}$, while in $MgCl_2$ and $MgSO_4$ is 61 mF $cm^{-2}$ and 24 mF $cm^{-2}$, respectively. Higher capacitance values indicate a higher percentage of doped structure units (see eqn (S1) and Table S2†), possibly due to a more facile anion association with the redox sites on the CPE-K backbone upon oxidation and transport within the bulk.[39] The $C_{Areal}$ values reported here are based on a higher applied current (10 mA $cm^{-2}$) than previous studies using similar CPE-K gels but with different electrolyte conditions. This emphasizes the importance of carefully selecting the electrolyte solution for optimal electrochemical response within the gels.

Among the electrolytes tested, NaCl possesses the higher diffusion coefficient ($D$) and is the stronger electrolyte (lower dissociation energy in water),[52] which may explain the higher $\langle I \rangle_p$ and $C_{areal}$ at every rate tested. At a given concentration, $MgCl_2$ has twice the number of anions ($Cl^-$) than $MgSO_4$ ($SO_4^{2-}$) to participate in anionic charge compensation. In addition, the Hofmeister series establishes that $SO_4^{2-}$ (kosmotrope) interacts more strongly with water than $Cl^-$ (chaotrope) due to the more localized valence charge binding strongly with water molecules.[53,54] We hypothesize that $Cl^-$ anions in $MgCl_2$ exhibit improved transport and association with the redox-active site of CPE-K compared to $SO_4^{2-}$ in $MgSO_4$, echoing the greater $C_{areal}$ observed (close to that in NaCl). Furthermore, the lower $C_{Areal}$ with $MgSO_4$ could also result from additional steric effects due to the $SO_4^{2-}$ size and larger solvation shell.[55–57] That $Na^+$ has a lower charge density and higher ligand exchange rates relative to that of $Mg^{2+}$ may also contribute to the higher $C_{areal}$ of the gels with NaCl over $MgCl_2$, as $Cl^-$ are more readily available in NaCl than in $MgCl_2$.[58,59] This analysis is further supported by trends in $IR_{drop}$ determined from the GCD curves, see Fig. S6.† For instance, the $IR_{drop}$ obtained from the GCD curves of the gels in 2 M NaCl electrolytes (2 mV) is 2-times and 4-times smaller than those for the gels in 2 M $MgCl_2$ electrolytes (4 mV) and 2 M $MgSO_4$ electrolytes (8 mV), respectively, indicating lower internal and electrolyte diffusion resistance.[60] All gels retained over 95% of their capacitance over 10 000 cycles when tested at $\langle J \rangle$ = 10 mA $cm^{-2}$ regardless of the electrolyte, see Fig. 2D, thereby demonstrating excellent stability.

After determining the effect of the electrolyte on the pseudocapacitive performance of CPE-K gels, we sought to understand ion transport. Quantitative information was obtained by analyzing the log–log plot of the $\langle I \rangle_p$ from the CV (Fig. 3A–C) measurements *vs.* scan rates ($\nu$), as summarized in Fig. 3D, S7,† and Table 2. Fig. 3D illustrates the power law in eqn (2):[61,62]

$$\langle I \rangle p \propto \nu^b \quad (2)$$

where the slope of the linear fit of the log–log plot corresponds to $b$. Note that CPE-K gels yield an increasing $b$ value from 0.88 to 0.91 and 0.95 in $MgSO_4$, $MgCl_2$, and NaCl, respectively, at scan rates ≤ 100 mV $s^{-1}$. These $b$ values, close to unity, indicate a mechanism mostly dominated by surface adsorption events for low scan rates before diffusion becomes limiting. These results align with typical pseudocapacitive behavior, as pseudocapacitors are kinetically limited at low scan rates only by surface faradaic reactions and bulk electrolyte diffusion at higher scan rates.[61–64]

Electrochemical impedance spectroscopy (EIS) from 100 kHz to 100 mHz was used to understand the electrochemical behavior in different electrolytes, particularly charge transfer resistances and ionic mobility. The resulting Nyquist plots were fitted to a modified equivalent Randles circuit and, when appropriate, complemented with an additional Warburg impedance ($W$) to account for diffusion effects (Fig. S8†). The resulting circuit accommodates the ~45° diffusion-controlled electrochemical response detected at low frequencies. This approach gave the simplest equivalent circuit $R_S + (Q_{geom}/R_{CT}) + W$, where $R_s$ is the series resistance, $Q_{geom}$ stands for constant phase element, and $R_{CT}$ represents the charge transfer resistance.[8,32,65] No evident semi-circles were observed from the Nyquist plots of the gels in NaCl and $MgCl_2$, but a sizable charge transfer resistance ($R_{CT}$) of ~1.5 Ω was obtained when gels were immersed in $MgSO_4$, as shown in Fig. 3E and Table 2. The sizable $R_{CT}$ of the gels in $MgSO_4$ aligns with our hypothesis

 

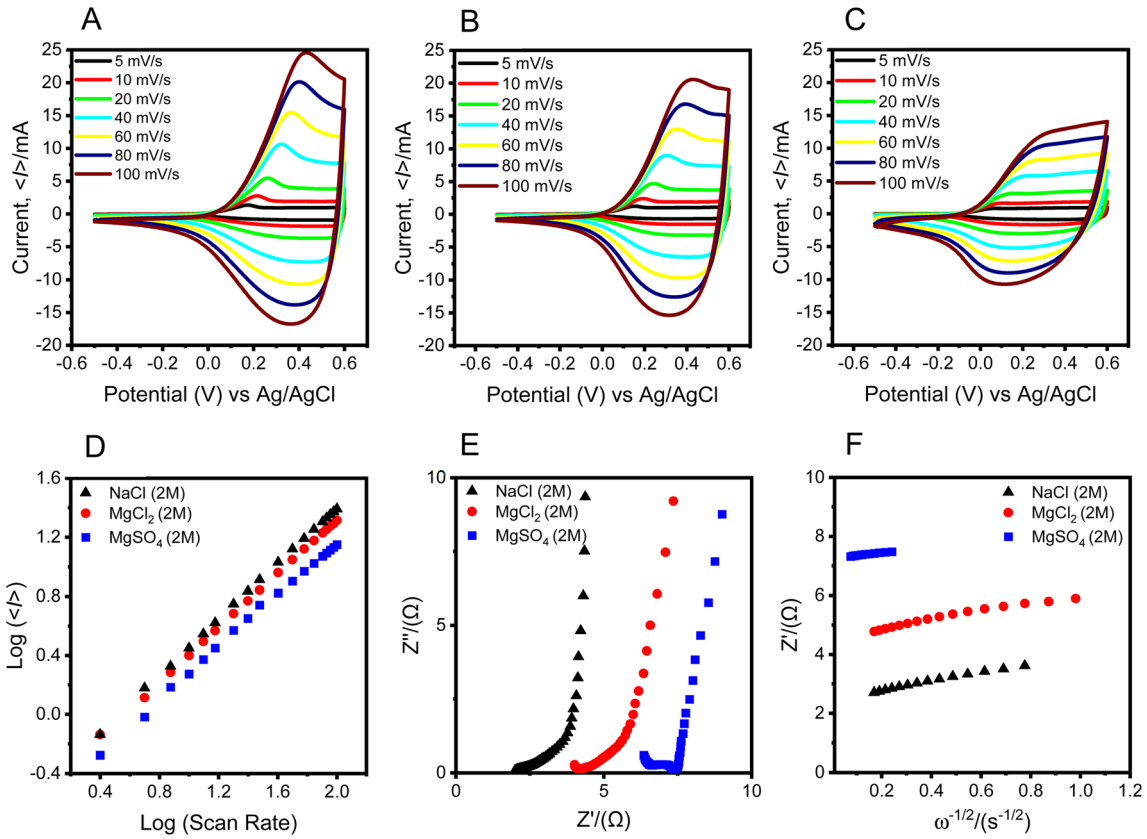


Fig. 3 Scan-rate dependent CV traces of CPE-K gels with $d_{Thk} = 250$ μm in (A) 2 M NaCl, (B) 2 M $MgCl_2$, and (C) 2 M $MgSO_4$ electrolyte solutions; (D) log–log plot of peak current *vs.* scan rate comparison of CPE-K gels in each electrolyte; (E) Nyquist-plot comparison of the CPE-K gels and (F) the relationship of $Z'$ and $\omega^{-1/2}$ of the investigated systems for determining the Warburg factor in the different electrolyte solutions, both obtained *via* electrochemical impedance spectroscopy (EIS). Measurements were carried out under ambient conditions.

Table 2 Characterization of CPE-K gels ($d_{Thk} = 250$ μm) in different electrolyte solutions[a]

| Electrolyte (2 M) | $G'$ (kPa) | $D^{52}$ ($cm^2\ s^{-1}$) | CE (%) | Stability[b] (10 k cycles) | $b \leq 100$ | $R_{CT}$ (Ω) | $\sigma$ ($\Omega\ s^{-1/2}$) | $\alpha$ | ESR (Ω) |
|---|---|---|---|---|---|---|---|---|---|
| NaCl | 34 | $1.6 \times 10^{-5}$ | 100 | >95% | 0.95 | <1 | 1.50 | 0.24 | 4 |
| $MgCl_2$ | 38 | $1.1 \times 10^{-5}$ | 99 | >95% | 0.91 | <1 | 1.68 | 0.23 | 7 |
| $MgSO_4$ | 42 | $0.9 \times 10^{-5}$ | 98 | >95% | 0.88 | 1.5 | 0.96 | 0.22 | 10 |

[a] $G'$ = gel-like elastic modulus coefficient obtained from rheological measurements. $D$ = diffusion coefficient of the electrolyte. CE = coulombic efficiency. [b] Stability refers to the capacitance retention upon multiple cycles. $b$ = slope of the log–log plot of $\langle I \rangle$ *vs.* scan rate, $\sigma$ = Warburg factor, $\alpha$ = doping percentage of the polymeric backbone (*via* electrochemical charge compensation) determined at 0.25 A $g^{-1}$, and ESR = equivalent series resistance. All measurements were conducted in ambient conditions.

regarding ion transport in CPE-K and its corresponding smaller $C_{Areal}$ at higher rates.

Gels in NaCl have the lowest equivalent series resistances – ESR (~4 Ω), which corresponds to the overall series resistance of the system and includes the electronic resistances of the solution and electrodes, the contact resistance, and ion diffusion resistance (determined by extrapolating the vertical portion of the Nyquist plot to the real axis).[32,66] In all cases, the – ESR reported here are lower than those reported in previous studies using similar CPE-K gels but with electrolyte solutions with lower ionic concentrations.[2,32] That the Nyquist plot for the gels in NaCl becomes more vertical at higher frequencies indicates a closer approximation to ideal capacitive behavior for CPE-K in this electrolyte.[3] This observation was further verified by determining the Warburg factor ($\sigma$) of the gels using eqn (3):

$$Z' = R_E + R_{CT} + \sigma\omega^{-1/2} \quad (3)$$

where $R_E$ is the resistance between the electrolyte and the electrode, $R_{CT}$ is the charge transfer resistance, and $\omega$ is the angular frequency, see Fig. 3F and S9.† [67] Note that gels exhibited a similar $\sigma$ value in NaCl (1.5 $\Omega\ s^{-0.5}$) and $MgCl_2$ (1.7 $\Omega\ s^{-0.5}$), in line with their similar performances. However, the ideal capacitive behavior for the gels in NaCl starts at a higher

frequency (1.6 Hz) than that for gels in $MgCl_2$ (1.0 Hz). These results indicate that the CPE-K gels in NaCl benefit from faster ionic diffusion kinetics,[3,10,62] in line with our previous analysis regarding NaCl higher diffusion coefficient ($D$) and lower dissociation energy in water than the other investigated electrolytes ($MgCl_2$ and $MgSO_4$). Altogether, these data suggest that the CPE-K gels benefit from higher ionic diffusion within its 3D conductive network in NaCl electrolyte, allowing for enhanced ionic–electronic coupling response of the CPE-K redox-active sites during cycling.[2,10,32,66] Therefore, it is reasonable to concentrate on using NaCl electrolytes for all subsequent investigations.

It was of interest to understand the influence of gel thickness on electrochemical performances. We examined the scalability of the gel capacitance as a function of $d_{Thk}$ (250 μm, 500 μm, 750 μm, and 1250 μm, obtained from incremental mass loading, see Methods) from the charge-collecting Au electrode surface. As shown in Fig. 4A, all gels maintained their pseudocapacitive nature with increasing thickness, as illustrated by their quasi-rectangular CV curves (5 mV $s^{-1}$).[4,6,32] GCD measurements at $\langle J \rangle = 0.5$ mA $cm^{-2}$ reveal that the $C_{Areal}$ of the gels scales proportionally with $d_{Thk}$, see Fig. 4B and Table S3.† Specifically, increasing $d_{Thk}$ from 250 μm to 1250 μm increases $C_{Areal}$ from 92 mF $cm^{-2}$ to 523 mF $cm^{-2}$. The $C_{Areal}$ value for $d_{Thk} = 1250$ μm is 1.9 times larger than that reported for the single-component binder-free CPHs based on PANI, as shown in Table 1.[22,29,68–70] It is important to note that the specific capacitance (F $g^{-1}$) of the hydrogels remains with a similar value when increasing $d_{Thk}$ for specific current <0.5 A $g^{-1}$, see Table S4.† That the value of the specific capacitance at <0.5 A $g^{-1}$ of the hydrogels remains similar when increasing $d_{Thk}$ agrees with the increment of $C_{Areal}$, as the charge collecting surface remains the same in all cases. However, the specific capacitance of the gel is compromised at >0.5 A $g^{-1}$ upon increasing $d_{Thk}$, indicating that the thicker gels possess a lower EASA/gram than the thinner gels at high charging/discharging rates.

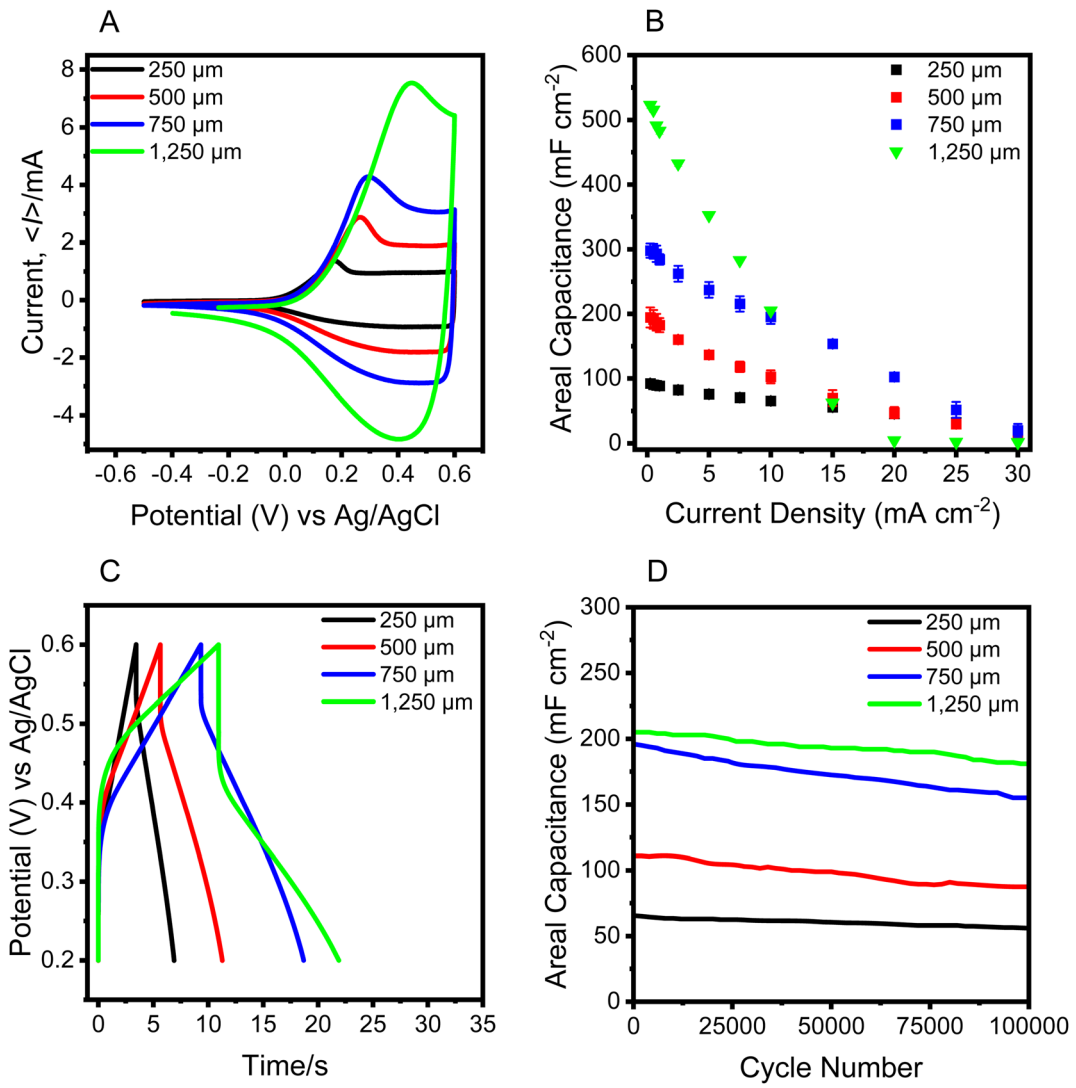


Fig. 4 Electrochemical characterization of 20 mg $mL^{-1}$ CPE-K gels with different $d_{Thk}$ in 2 M NaCl. (A) CV at 5 mV $s^{-1}$; (B) areal capacitance in mF $cm^{-2}$ at different $\langle J \rangle$; (C) charge/discharge curve at 7.5 mA $cm^{-2}$; (D) capacitance retention upon electrochemical charge/discharge cycles at 10 mA $cm^{-2}$. Measurements were carried out in ambient conditions.

 

The linear increase of $C_{Areal}$ with $d_{Thk}$ occurs at every rate tested (up to 30 mA cm$^{-2}$) up to $d_{Thk}$ = 750 μm, after which thicker gels exhibit smaller $C_{Areal}$ at high discharge rates (>10 mA cm$^{-2}$). For example, at 15 mA cm$^{-2}$, the gel with $d_{Thk}$ = 1250 (62 mF cm$^{-2}$) exhibits a similar $C_{areal}$ to those with $d_{Thk}$ = 250 μm (56 mF cm$^{-2}$) despite containing 5 times more CPE-K, see Fig. 4B and Table S3.† We then investigated the $d_{Thk}$ on the electrochemical reversibility of the CPE-K gels. The CE decreased from ~100% at $d_{Thk}$ = 250 μm to 96% at $d_{Thk}$ = 1250 μm, indicating a partial loss of electrochemical reversibility for thicker gels, see Fig. S10.† The corresponding CV traces show that increasing $d_{Thk}$ also results in anodic shifting of $\langle I \rangle_p$, associated with increased internal resistances.[2] This analysis is further supported by the trends in voltage loss ($IR_{drop}$) determined from the GCD curves taken at 1 mA cm$^{-2}$ (Fig. S11†) and 7.5 mA cm$^{-2}$ (Fig. 4C). For instance, the $IR_{drop}$ when $d_{Thk}$ = 1250 μm ($IR_{drop}$ ~25 mV) is ~12.5 times larger than that when $d_{Thk}$ = 250 μm ($IR_{drop}$ ~2 mV) for the same discharge rate of 1 mA cm$^{-2}$.

CPE-K gels are remarkably stable regardless of $d_{Thk}$, retaining over 85% of initial $C_{Areal}$ after 100 000 charge/discharge cycles ($C_{Areal\ 100K}$) even when operated at 10 mA cm$^{-2}$, see Fig. 4C and Table 2. These cycling stabilities outperform previously reported CPE-K gels in biocompatible media (Table 1), even though the measurements reported here were carried out at an applied current 10 times larger.[2,9,10] A possible reason for the increased stability may be the higher mechanical properties of the gel in NaCl, as the hydrogel keeps better its electrochemical integrity due to higher tolerance to volumetric changes upon cycling. Post-cycling CV characterization revealed only a minimal reduction in the pseudocapacitive window, see Fig. S12.† UV-vis absorption measurements of the CPE-K before and after conducting the cycling stability measurements revealed no noticeable wavelength shifts of the peaks nor changes to the relative contributions of neutral and polaronic states, implying no significant chemical degradation of the CPE-K chemical structure (Fig. S13†).

To gauge how diffusion limitations within the gel matrix contribute to the more pronounced $C_{Areal}$ decrease at higher cycling rates when $d_{Thk}$ approaches 1250 μm, we deconvoluted $C_{Areal}$ into fractional contributions from surface-controlled ($S_C$)

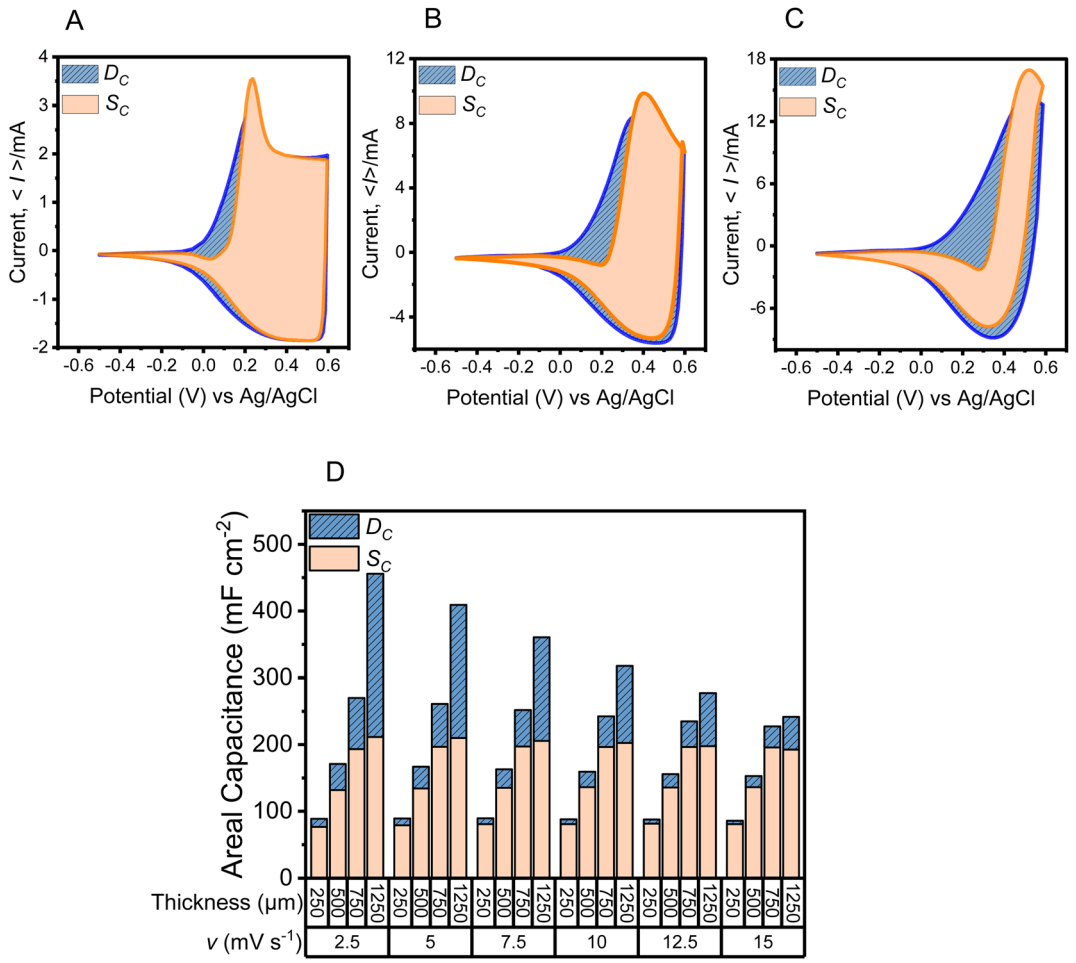


Fig. 5 CV representing the contributions from surface-controlled and diffusion-controlled processes determined following eqn (4) for different gel thicknesses: (A) 250 μm, (B) 750 μm, and (C) 1250 μm, all measured at 10 mV s$^{-1}$. (D) Fractional contributions of the $C_{Areal}$ corresponding to surface-controlled ($S_C$) and diffusion-controlled ($D_C$) pseudocapacitive behaviors at different rates for each thickness investigated. Measurements were carried out in ambient conditions.

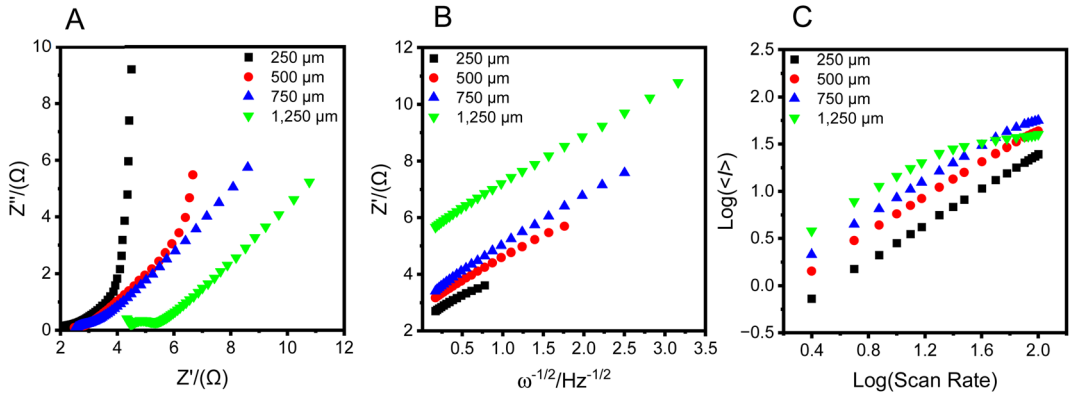


Fig. 6 (A) Nyquist-plot comparison of the CPE-K gels at different with different $d_{Thk}$ and (B) the relationship of $Z'$ and $\omega^{-1/2}$ of the same systems for determining the Warburg factor. (C) log–log plot of peak current *vs.* scan rate comparison for each $d_{Thk}$ investigated in NaCl (2 M). See Fig. S16† for raw measurements. Measurements were carried out in ambient conditions.

and diffusion-controlled ($D_C$) pseudocapacitive behavior following eqn (4):[1]

$$\langle I \rangle = k_1 v + k_2 v^{0.5} \quad (4)$$

where $\langle I \rangle$ is the current response at a given potential, $v$ corresponds to the scan rate during CV, and $k_1$ and $k_2$ correspond to the $\langle I \rangle$ contributions from $S_C$ and the $D_C$, respectively (see Fig. S14, 5A–D, and ESI† for more details). At low thicknesses $S_C$ governs $C_{Areal}$. For example, when $d_{Thk}$ = 250 µm and measurements are carried out at a rate of 2.5 mV s$^{-1}$, 87% of its total $C_{Areal}$ (88 mF cm$^{-2}$) corresponds to $S_C$, while 13% corresponds to $D_C$, see Fig. S15 and Table S5.† However, the fractional contribution to the total $C_{Areal}$ corresponding to $D_C$ increases with $d_{Thk}$. For example, when $d_{Thk}$ = 1250 µm, 56% (244 mF cm$^{-2}$) of the total $C_{Areal}$ (455 mF cm$^{-2}$) corresponds to $D_C$, while 46% (211.3 mF cm$^{-2}$) corresponds to $S_C$.

Upon increasing the cycling rate, the $C_{Areal}$ contribution corresponding to $S_C$ remains relatively constant at all $d_{Thk}$, while the contribution from $D_C$ decreases, see Fig. 5D. For example, the $C_{Areal}$ originating from $S_C$ in $d_{Thk}$ = 250 µm gels is 77 mF cm$^{-2}$ at 2.5 mV s$^{-1}$ and 80 mF cm$^{-2}$ at 15 mV s$^{-1}$, while for gels with $d_{Thk}$ = 1250 µm, is 211 mF cm$^{-2}$ and 193 mF cm$^{-2}$, respectively. Conversely, the $C_{Areal}$ corresponding to $D_C$ in $d_{Thk}$ = 250 µm gels decreases from 12 mF cm$^{-2}$ to 5 mF cm$^{-2}$ upon increasing the cycling rate, while for $d_{Thk}$ = 1250 µm, it decreases from 245 mF cm$^{-2}$ to 49 mF cm$^{-2}$. This analysis reveals that the decrease in $C_{Areal}$ at high $d_{Thk}$ upon increasing the charge/discharge rate is primarily due to ionic diffusion limitations. As a result, the redox-active sites of CPE-K gels with $d_{Thk}$ approaching 1250 µm are not fully accessible by anions when cycling at higher rates.[32,66]

EIS characterization revealed that increasing $d_{Thk}$ compromises the ideal capacitive behavior of the electrode, see Fig. 6A. For example, when $d_{Thk}$ = 250 µm, ideal capacitive behavior starts at 1.6 Hz and extends to 0.1 Hz (Fig. S17†). Contrarily, no ideal capacitive behavior is observed when $d_{Thk}$ = 1250 µm at the frequencies tested. In addition, Fig. 6B shows that the frequency range in the Warburg domain increases with gel thickness, echoing our previous CV analysis. Our current thinking is that increasing thickness requires more time for the ions to travel and associate with the redox active sites of CPE when $d_{Thk}$ increases. This feature becomes more apparent when $b$ is considered, as $b$ decreases from >0.88 to <0.6 when $d_{Thk}$ approaches 1250 µm, see Fig. 6C, S18,† and Table 3. Altogether, the increments in ESR, $b$, and the frequency range in the Warburg domain, along with the deviation of ideal capacitive behavior when $d_{Thk}$ = 1250 µm, explains its minimal $C_{Areal}$ at higher rates, as compromised ionic conductivity and increased internal resistances hampers the charge storing mechanism of the gel. These results are consistent with the increased contributions from $D_C$ processes upon increasing $d_{Thk}$, and are in alignment with the lower EASA/gram (∼specific capacitance; F g$^{-1}$) in thicker gels at high charging/discharging rates.[2,10,32,62]

Table 3 Electrochemical characterization of CPE-K gels with different thicknesses in 2 M NaCl[a]

| Hydrogel thickness ($d_{Thk}$) | CE (%) | Stability[b] (100 k cycles) | $b$ ≤ 100 (mV s$^{-1}$) | $R_{CT}$ (Ω) | $\sigma$ (Ω s$^{-1/2}$) | ESR (Ω) | $C_{Areal\ 100K}$ (mF cm$^{-2}$) |
|---|---|---|---|---|---|---|---|
| 250 µm | 100 | >85% | 0.95 | <1 | 1.50 | 4 | 56 |
| 500 µm | 99 | >85% | 0.91 | <1 | 1.59 | 6.5 | 88 |
| 750 µm | 98 | >85% | 0.88 | <1 | 1.77 | 8.5 | 155 |
| 1250 µm | 97 | >85% | <0.6 | 1.5 | 1.69 | 12.5 | 180 |

[a] CE = coulombic efficiency at 5 mV s$^{-1}$. [b] Stability refers to the capacitance retention upon multiple cycles, $b$ = slope of the log–log plot of $\langle I \rangle$ *vs.* scan rate, $R_{CT}$ = charge transfer resistance, $\sigma$ = Warburg factor, ESR = equivalent series resistances, and $C_{Areal\ 100K}$ = the areal capacitance of the investigated systems after 100 000 cycles.

 

## 3. Conclusions

We have shown that using 2 M NaCl electrolyte improves the $C_{Areal}$ of CPE-K gels, as anions ($Cl^-$) are readily available in NaCl to participate in the pseudocapacitive process over the conventional electrolytes $MgCl_2$ and $MgSO_4$, without significantly compromising mechanical properties and robustness. We further demonstrated that it is possible to scale up the $C_{Areal}$ of CPE-K gels with $d_{Thk}$ in 2 M NaCl electrolyte solutions, providing an attractive approach to improve charge storage with a given charge-collecting electrode area. Specifically, gels with $d_{Thk} = 1250$ μm possess $C_{Areal}$ (523 mF $cm^{-2}$) five times higher than those with $d_{Thk} = 250$ μm (92 mF $cm^{-2}$) when determined at 0.5 mA $cm^{-2}$. In addition, this value is 1.9 times larger than that for single-component binder-free CPHs, see Table 1. The electrode with $d_{Thk} = 1250$ μm can still be operated at a rate of 15 mA $cm^{-2}$, with $C_{Areal} = 60$ mF $cm^{-2}$. Electrochemical characterization revealed that the charge storage mechanism is dominated by surface-controlled events at low rates, while diffusion limitations become more prominent at high rates. We further show that it is possible to maintain efficient ion transport within the CPE-K gels up to a critical thickness of 750 mm, after which, for thicker gels, diffusion-controlled mechanisms limit the performances at higher rates as observed by the lower EASA/gram (~specific capacitance; F $g^{-1}$). CPE-K gels can achieve excellent cycling stability, retaining over 86% of their initial capacitance after 100 000 cycles, even at 10 mA $cm^{-2}$, regardless of $d_{Thk}$. Such cycling stabilities were achieved due to their superior mechanical strength in 2 M NaCl relative to previously examined electrolytes.[2,9] To our knowledge, the $C_{Areal}$ and cycling stabilities reported here are higher than those reported for state-of-the-art single-component CPH (Table 1). Altogether, these results suggest that creating thicker CPE-K gels is a relevant approach for storing and delivering charges at a slow rate, while thinner gels might be beneficial for storing and providing charges at higher rates. We envision that our work will stimulate the consideration of self-doped CPE gels for enabling electrochemical energy storage and conversion technologies.

## Author contributions

Vázquez, Quek, and Bazan conceptualized the idea, designed the experiments, and co-wrote the manuscript. Vázquez and Quek synthesized and structurally characterized the compounds. McCuskey, Yan, Peng, Ohayon, and Wang contributed with in-depth CV and EIS analysis pertinent to ion conductivity. All authors proofread the manuscript. Kundukad did the rheological measurements. Vázquez and Quek contributed equally to this work.

## Conflicts of interest

The authors declare no conflict of interest.

## Acknowledgements

This research was supported by the Ministry of Education, Singapore, under its Research Centre of Excellence award to the Institute for Functional Intelligent Materials (I-FIM, project No. EDUNC-33-18-279-V12) and by the National University of Singapore start-up grant A-0004525-00-00. Work at SCELSE was supported by core research funds, SCELSE is funded by the National Research Foundation, Ministry of Education, Nanyang Technological University (NTU), and National University of Singapore (NUS) and hosted by NTU in partnership with NUS.

## References

1 K. Li, X. Wang, S. Li, P. Urbankowski, J. Li, Y. Xu and Y. Gogotsi, *Small*, 2020, **16**, 1906851.
2 R. J. Vázquez, G. Quek, S. R. McCuskey, L. Llanes, B. Kundukad, X. Wang and G. C. Bazan, *J. Mater. Chem. A*, 2022, **10**, 21642–21649.
3 X. Wang, S.-M. Bak, M. Han, C. E. Shuck, C. McHugh, K. Li, J. Li, J. Tang and Y. Gogotsi, *ACS Energy Lett.*, 2022, **7**, 30–35.
4 T. S. Mathis, N. Kurra, X. Wang, D. Pinto, P. Simon and Y. Gogotsi, *Adv. Energy Mater.*, 2019, **9**, 1902007.
5 S. K. Simotwo, C. Delre and V. Kalra, *ACS Appl. Mater. Interfaces*, 2016, **8**, 21261–21269.
6 S. Fleischmann, J. B. Mitchell, R. Wang, C. Zhan, D. Jiang, V. Presser and V. Augustyn, *Chem. Rev.*, 2020, **120**, 6738–6782.
7 X. Yu, S. Yun, J. S. Yeon, P. Bhattacharya, L. Wang, S. W. Lee, X. Hu and H. S. Park, *Adv. Energy Mater.*, 2018, **8**, 1–33.
8 J. Wang, S. Dong, B. Ding, Y. Wang, X. Hao, H. Dou, Y. Xia and X. Zhang, *Natl. Sci. Rev.*, 2017, **4**, 71–90.
9 G. Quek, Y. Su, R. K. Donato, R. J. Vázquez, V. S. Marangoni, P. R. Ng, M. C. F. Costa, B. Kundukad, K. S. Novoselov, A. H. C. Neto and G. C. Bazan, *Adv. Electron. Mater.*, 2022, **8**, 2100942.
10 G. Quek, B. Roehrich, Y. Su, L. Sepunaru and G. C. Bazan, *Adv. Mater.*, 2022, **34**, 2104206.
11 K. C. S. Lakshmi, X. Ji, T.-Y. Chen, B. Vedhanarayanan and T.-W. Lin, *J. Power Sources*, 2021, **511**, 230434.
12 J. F. Ponder, A. M. Österholm and J. R. Reynolds, *Chem. Mater.*, 2017, **29**, 4385–4392.
13 T. Liu and Y. Li, *InfoMat*, 2020, **2**, 807–842.
14 X. Chen, W.-Y. Tung, K. Yang, Y.-M. Chen, K. Liu, C.-F. Cheng and Y. Zhu, *ACS Appl. Polym. Mater.*, 2019, **1**, 1634–1640.
15 A. M. Bryan, L. M. Santino, Y. Lu, S. Acharya and J. M. D'Arcy, *Chem. Mater.*, 2016, **28**, 5989–5998.
16 F. N. Ajjan, Z. Khan, S. Riera-Galindo, S. Lienemann, M. Vagin, I. Petsagkourakis, R. Gabrielsson, S. Braun, M. Fahlman, O. Inganäs, M. Berggren and X. Crispin, *Adv. Energy Sustainability Res.*, 2020, **1**, 2000027.
17 S. Ghosh and O. Inganäs, *Adv. Mater.*, 1999, **11**, 1214–1218.
18 M. Zhang, Q. Zhou, J. Chen, X. Yu, L. Huang, Y. Li, C. Li and G. Shi, *Energy Environ. Sci.*, 2016, **9**, 2005–2010.
19 Y. Li, S. Park, K. Sarang, H. Mei, C.-P. Tseng, Z. Hu, D. Zhu, X. Li, J. Lutkenhaus and R. Verduzco, *ACS Polym. Au*, 2023, **3**, 267–275.
20 S. Sardana, A. Gupta, K. Singh, A. S. Maan and A. Ohlan, *J. Energy Storage*, 2022, **45**, 103510.

21 K. Liu, S. Wei, L. Song, H. Liu and T. Wang, *J. Agric. Food Chem.*, 2020, **68**, 7269–7280.
22 M. Moussa, M. F. El-Kady, D. Dubal, T. T. Tung, M. J. Nine, N. Mohamed, R. B. Kaner and D. Losic, *ACS Appl. Energy Mater.*, 2020, **3**, 923–932.
23 J. Li, W. Yan, G. Zhang, R. Sun and D. Ho, *J. Mater. Chem. C*, 2021, **9**, 1685–1692.
24 S. Sardana, A. Gupta, K. Singh, A. S. Maan and A. Ohlan, *J. Energy Storage*, 2022, **45**, 103510.
25 L. Li, Y. Wang, X. Bao, D. H. Nguyen, C. Zhang and T. Liu, *Chem. Eng. J.*, 2023, **452**, 139223.
26 A. Mir, A. Kumar and U. Riaz, *RSC Adv.*, 2022, **12**, 19122–19132.
27 D. Zhang, Y. Chen, X. Yu, H. Huang, L. Li and L. Wei, *Mater. Res. Express*, 2019, **6**, 085044.
28 M. Samtham, D. Singh, K. Hareesh and R. S. Devan, *J. Energy Storage*, 2022, **51**, 104418.
29 K. Namsheer and C. S. Rout, *RSC Adv.*, 2021, **11**, 5659–5697.
30 G. Quek, R. J. Vázquez, S. R. McCuskey, B. Kundukad and G. C. Bazan, *Adv. Mater.*, 2022, 2203480.
31 S. P. O. Danielsen, B. J. Thompson, G. H. Fredrickson, T.-Q. Nguyen, G. C. Bazan and R. A. Segalman, *Macromolecules*, 2022, **55**, 3437–3448.
32 Y. Su, S. R. McCuskey, D. Leifert, A. S. Moreland, L. Zhou, L. C. Llanes, R. J. Vazquez, L. Sepunaru and G. C. Bazan, *Adv. Funct. Mater.*, 2021, **31**, 2007351.
33 R. J. Vázquez, S. R. McCuskey, G. Quek, Y. Su, L. Llanes, J. Hinks and G. C. Bazan, *Macromol. Rapid Commun.*, 2022, **43**, 2100840.
34 S. R. McCuskey, Y. Su, D. Leifert, A. S. Moreland and G. C. Bazan, *Adv. Mater.*, 2020, **32**, 1908178.
35 D. Yang, *Chem. Mater.*, 2022, **34**, 1987–1989.
36 K. Wang, X. Zhang, C. Li, H. Zhang, X. Sun, N. Xu and Y. Ma, *J. Mater. Chem. A*, 2014, **2**, 19726–19732.
37 S. P. O. Danielsen, G. E. Sanoja, S. R. McCuskey, B. Hammouda, G. C. Bazan, G. H. Fredrickson and R. A. Segalman, *Chem. Mater.*, 2018, **30**, 1417–1426.
38 T. Liu, L. Finn, M. Yu, H. Wang, T. Zhai, X. Lu, Y. Tong and Y. Li, *Nano Lett.*, 2014, **14**, 2522–2527.
39 K. D. Fong, T. Wang and S. K. Smoukov, *Sustainable Energy Fuels*, 2017, **1**, 1857–1874.
40 L. Pan, G. Yu, D. Zhai, H. R. Lee, W. Zhao, N. Liu, H. Wang, B. C. K. Tee, Y. Shi, Y. Cui and Z. Bao, *Proc. Natl. Acad. Sci. U. S. A.*, 2012, **109**, 9287–9292.
41 L. Zhang, Y. Wu, Y. Xia and L. Jin, *Electrochim. Acta*, 2022, **412**, 140108.
42 Q. Zhou, W. Teng, Y. Jin, L. Sun, P. Hu, H. Li, L. Wang and J. Wang, *Electrochim. Acta*, 2020, **334**, 135530.
43 Q. Liu, J. Qiu, C. Yang, L. Zang, G. Zhang and E. Sakai, *Adv. Mater. Technol.*, 2021, **6**, 2000919.
44 C. Hu, Y. Lin, J. W. Connell, H. M. Cheng, Y. Gogotsi, M. M. Titirici and L. Dai, *Adv. Mater.*, 2019, **31**, 1–14.
45 P. Simon and Y. Gogotsi, *Mater. Sustainable Energy*, 2010, **7**, 138–147.
46 P. Stoodley, Z. Lewandowski, J. D. Boyle and H. M. Lappin-Scott, *Biotechnol. Bioeng.*, 1999, **65**, 83–92.
47 A. I. Van Den Bulcke, B. Bogdanov, N. De Rooze, E. H. Schacht, M. Cornelissen and H. Berghmans, *Biomacromolecules*, 2000, **1**, 31–38.
48 B. Kundukad, T. Seviour, Y. Liang, S. A. Rice, S. Kjelleberg and P. S. Doyle, *Soft Matter*, 2016, **12**, 5718–5726.
49 O. Diaz-Morales, F. Calle-Vallejo, C. De Munck and M. T. M. Koper, *Chem. Sci.*, 2013, **4**, 2334–2343.
50 Q. Wei, Q. Li, Y. Jiang, Y. Zhao, S. Tan, J. Dong, L. Mai and D.-L. Peng, *Nanomicro Lett.*, 2021, **13**, 55.
51 G. Choi, J. Kim and B. Kang, *Chem. Mater.*, 2019, **31**, 6097–6104.
52 R. W. Holloway, R. Maltos, J. Vanneste and T. Y. Cath, *J. Membr. Sci.*, 2015, **491**, 121–131.
53 A. P. dos Santos, A. Diehl and Y. Levin, *Langmuir*, 2010, **26**, 10778–10783.
54 A. Salis and B. W. Ninham, *Chem. Soc. Rev.*, 2014, **43**, 7358–7377.
55 J. Teychené, H. R. Balmann, L. Maron and S. Galier, *J. Mol. Liq.*, 2019, **294**, 111394.
56 R. D. Mountain, *Int. J. Thermophys.*, 2007, **28**, 536–543.
57 A. Kundu, S. I. Mamatkulov, F. N. Brünig, D. J. Bonthuis, R. R. Netz, T. Elsaesser and B. P. Fingerhut, *ACS Phys. Chem. Au*, 2022, **2**, 506–514.
58 S. Huang, P. Du, C. Min, Y. Liao, H. Sun and Y. Jiang, *J. Fluoresc.*, 2013, **23**, 621–627.
59 M. Remko, D. Fitz and B. M. Rode, *Amino Acids*, 2010, **39**, 1309–1319.
60 H. Gul, A.-H. A. Shah, U. Krewer and S. Bilal, *Nanomaterials*, 2020, **10**, 118.
61 J. C. Russell, V. A. Posey, J. Gray, R. May, D. A. Reed, H. Zhang, L. E. Marbella, M. L. Steigerwald, Y. Yang, X. Roy, C. Nuckolls and S. R. Peurifoy, *Nat. Mater.*, 2021, **20**, 1136–1141.
62 V. Augustyn, J. Come, M. A. Lowe, J. W. Kim, P.-L. Taberna, S. H. Tolbert, H. D. Abruña, P. Simon and B. Dunn, *Nat. Mater.*, 2013, **12**, 518–522.
63 B. E. Conway, *Proc. Int. Power Sources Symp.*, 1991, 319–327.
64 V. Augustyn, P. Simon and B. Dunn, *Energy Environ. Sci.*, 2014, **7**, 1597.
65 H. Li, J. Wang, Q. Chu, Z. Wang, F. Zhang and S. Wang, *J. Power Sources*, 2009, **190**, 578–586.
66 F. Béguin, V. Presser, A. Balducci and E. Frackowiak, *Adv. Mater.*, 2014, **26**, 2219–2251.
67 W. Liu, H. Yi, Q. Zheng, X. Li and H. Zhang, *J. Mater. Chem. A*, 2017, **5**, 10928–10935.
68 J. Rivnay, P. Leleux, M. Ferro, M. Sessolo, A. Williamson, D. A. Koutsouras, D. Khodagholy, M. Ramuz, X. Strakosas, R. M. Owens, C. Benar, J. M. Badier, C. Bernard and G. G. Malliaras, *Sci. Adv.*, 2015, **1**, 1–6.
69 H. Zhou, G. Han, Y. Xiao, Y. Chang and H.-J. Zhai, *J. Power Sources*, 2014, **263**, 259–267.
70 T. P. Anandhu, R. R. Mohan, J. Cherusseri, R. Rohith and S. J. Varma, *Electrochim. Acta*, 2022, **425**, 140740.

 